

**Pt<sub>80</sub>Fe<sub>20</sub> surface from first principles: Electronic structure and adsorption of CO and atomic H**Robin Hirschl,<sup>1,2,\*</sup> Françoise Delbecq,<sup>1</sup> Philippe Sautet,<sup>1</sup> and Jürgen Hafner<sup>2</sup><sup>1</sup>*Institut de Recherches sur la Catalyse, CNRS, 2 Avenue Albert Einstein, F-69626 Villeurbanne Cedex, France and Ecole Normale Supérieure de Lyon, 46 Allée d'Italie, F-69364 Lyon Cedex 07, France*<sup>2</sup>*Institut für Materialphysik and Center for Computational Materials Science, Universität Wien, Sensengasse 8/12, A-1090 Wien, Austria*

(Received 22 May 2002; published 31 October 2002)

The electronic structure and the local adsorption properties of the Pt<sub>80</sub>Fe<sub>20</sub> (111) alloy surface have been theoretically studied in comparison to a pure Pt (111) surface in the framework of spin-density-functional theory. Pt-based alloys are important catalysts for the production of unsaturated alcohols. According to several experimental determinations of the surface composition, the surface is modeled by a Pt<sub>3</sub>Fe bulk alloy terminated by a single layer of pure Pt. Test adsorbates are CO and atomic hydrogen. Iron atoms bond strongly to neighboring Pt atoms, thereby shifting their *d* bands toward higher binding energies and reducing their chemical reactivity. The site dependence of those effects could be resolved by evaluating the partial densities of states of individual *d*-band orbitals. Though only iron atoms carry a magnetic moment, spin polarization is qualitatively important. In a second step we investigated the influence of iron atoms in the surface layer, using Pt<sub>3</sub>Fe (111) as a test surface. Here an additional effect of local strain adds to the electronic changes through heteroatomic bonds.

DOI: 10.1103/PhysRevB.66.155438

PACS number(s): 68.43.Bc, 73.20.At, 68.47.De

**I. INTRODUCTION**

It is well known that alloy surfaces might exhibit electronic, chemical, and catalytic properties that are considerably different from the pure surfaces of the constituting elements. Platinum-based alloys, e.g., PtFe and PtSn, have shown to be very selective for the hydrogenation of  $\alpha$ ,  $\beta$ -unsaturated aldehydes to unsaturated alcohols, important ingredients for many processes in fine chemistry.<sup>1-4</sup> The unsaturated aldehydes present two adjacent double bonds in conjugation, C=O and C=C. While over pure Pt surfaces primarily the C=C double bond is hydrogenated, alloying with promoting elements shifts the ratio towards the predominant hydrogenation of the C=O bond.

The present study aims at understanding the electronic structure of the Pt<sub>80</sub>Fe<sub>20</sub> (111) alloy surface and its interaction with small adsorbates as a first step towards the explanation of the selectivity of the alloy catalyst. It extends a previous qualitative theoretical work by two of the authors using the semiempirical extended Hückel method.<sup>5</sup> As probe adsorbates, we have again chosen carbon monoxide and atomic hydrogen. The former plays an important role in the characterization of surface properties since it is frequently used as a probe molecule.<sup>6</sup> The latter is not only the simplest possible adsorbate but also one of the reactants in the hydrogenation reaction and therefore of relevance. The properties of both species on Pt<sub>80</sub>Fe<sub>20</sub> (111) single-crystal surfaces have been investigated experimentally.<sup>7,8</sup>

The alloy surface under investigation in this work has been studied extensively experimentally. Low-energy electron-diffraction (LEED),<sup>9</sup> x-ray photoemission core-level spectroscopy, (Ref. 10) and low-energy ion scattering (LEIS)<sup>11</sup> results have been published. All of them confirm a large segregation of Pt towards the surface. The model geometry consequently consists of an ordered Pt<sub>3</sub>Fe com-

pound terminated by a single layer of pure Pt. The random replacement of further Fe atoms by Pt in the bulk necessary to obtain the correct stoichiometry is neglected. The (111) surface of this alloy displays only one atom type on two nonequivalent positions distinguished by the existence or nonexistence of an Fe nearest neighbor in the subsurface layer, respectively. Although all atoms of the surface layer are nonmagnetic, the magnetism of the Fe atoms plays an essential role for the qualitative description of the surface electronic structure.

Our results are obtained from first-principles calculations based on local spin-density-functional theory.<sup>12,13</sup> Section II describes the key-features of our calculations. After a discussion of the relaxation and the magnetic configuration of the alloy surface in Sec. III, we discuss in detail its local electronic structure in Sec. IV. Results on the geometry and energetics of our test adsorbates are presented in Sec. V. We include test calculations on the influence of possible Fe impurities in the surface layer on the adsorbates. In Sec. VI we discuss the electronic effects that lead to the changes in the adsorption energies and position our results in the framework of experiments. Finally, in Sec. VII some concluding remarks are presented.

A forthcoming article will compare adsorption modes of simple  $\alpha$ ,  $\beta$ -unsaturated aldehydes on Pt<sub>80</sub>Fe<sub>20</sub>. This will link the present work with a recently published article by Delbecq and Sautet discussing the adsorption of aldehydes on the pure Pt (111) surface.<sup>14</sup>

**II. METHODOLOGY**

Ground-state energies, surface relaxations, adsorption geometries, and electronic structure have been determined in the framework of local spin-density-functional theory. The single-particle Kohn-Sham equations were solved using the plane-wave-based Vienna *ab initio* simulation package

(VASP).<sup>15–18</sup> Their self-consistent solutions, corresponding to the electronic ground state, are found via the use of an iterative unconstrained band-by-band matrix-diagonalization scheme based on a residual minimization method.<sup>18,19</sup> Corrections to a purely local treatment of the exchange-correlation potential and energy were implemented by applying the generalized gradient approximation as proposed by Perdew and Wang (PW91).<sup>20</sup> Brillouin-zone sampling is performed on Monkhorst-Pack special points,<sup>21</sup> utilizing a generalized Gaussian smearing for integration in reciprocal space. The plane-wave energy cutoff is determined by the adsorbate potentials to be 400 eV for all calculations (unless otherwise stated below) and the  $k$ -point mesh was selected to correspond to  $(12 \times 12 \times 1)$   $k$  points in the primitive  $(1 \times 1)$  surface cell. These choices guarantee a sufficient convergence with respect to the energy cutoff and the number of  $k$  points.

The electron-ion interaction is described by the projector-augmented wave (PAW) method of Blöchl,<sup>22</sup> as further improved by Kresse and Joubert.<sup>23</sup> This approach is essentially an all-electron method, which improves the description of transition metals compared to the use of pseudopotentials. Pseudization radii are 1.32 and 1.16 Å for Pt and Fe, respectively, and the  $3p$  states of iron are treated as valence states to guarantee a good transferability of the potential.

The slab geometry of our calculated surface consists of four layers of substrate separated by four to six layers of vacuum. Four substrate layers are sufficient for close-packed fcc (111) surfaces. Adsorbates are introduced on one side of the surface only. For details of the surface model see Sec. III below. Ionic relaxation of the topmost surface layers is performed using a quasi-Newton algorithm to minimize the exact Hellmann-Feynman forces<sup>24</sup> acting on the atoms. Convergence checks were carried out regarding the thickness of the slab-separating vacuum.

Electronic densities of states (DOS) are obtained for individual atoms (local DOS) as well as for their single atomic orbitals (partial DOS) by projecting the plane-wave expanded wave functions onto spherical harmonics that are nonzero within a sphere around each ion. The radii were chosen such that the total numbers of electrons within the orbitals are more or less equal to the numbers of valence electrons included in the potential. However, neither the local nor the partial DOS change qualitatively when varying those radii within a reasonable range.

Since second partial derivatives of the energy are not yet implemented in VASP, the determination of stretching frequencies requires a numerical exploration of the potential-energy surface. A full vibrational spectrum of an adsorbate can be obtained by numerically approximating the Hessian matrix using finite differences and evaluating its eigenvalues. This approach only neglects the coupling of the adsorbate vibrations to the surface phonons, a reasonable omission since the former are of much higher frequency than the latter. For the highest adsorbate frequency (stretching of the intermolecular bond in CO and vibration along the  $z$  axis for H) it is even sufficient to calculate only the distance dependence of the energy in the single dimension of the configuration space corresponding to the vibration of interest. The har-

monic frequency as well as anharmonic corrections can be determined by fitting to a Morse potential developed to third order. The justification of the neglect of the highest frequency's coupling to other adsorbate vibrations lies in the excellent agreement of the frequencies obtained by either of the two methods. At very high coverages the decoupling of the highest vibrational frequency is likely to break down and even concerted vibrations of adjacent adsorbates might emerge.<sup>25</sup>

### III. CLEAN SURFACE COMPOSITION AND RELAXATION

$\text{Pt}_x\text{Fe}_{1-x}$  bulk alloys with about 75 at. % Pt crystallize in the ordered fcc  $L1_2$  ( $\text{AuCu}_3$ ) structure below the transition temperature of about 1500 K. At room temperature this phase is stable for platinum concentrations in the range  $60\% < x_{\text{Pt}} < 85\%$ .

As mentioned in the Introduction, the  $\text{Pt}_{80}\text{Fe}_{20}$  (111) alloy surface has been studied extensively experimentally. First, LEED investigations by Beccat *et al.*<sup>9</sup> already showed a strong segregation of Pt towards the surface. Their optimum model yielded  $96 \pm 4$ ,  $88 \pm 7$ , and  $85 \pm 15$  at. % of Pt in the uppermost three surface layers, respectively. This monotonous decrease of Pt content towards its bulk value is in contrast to  $\text{Pt}_x\text{Ni}_{1-x}$  alloys that exhibit an oscillatory concentration profile. For example, in the  $\text{Pt}_{78}\text{Ni}_{22}$  (111) alloy surface the first layer is almost purely built from Ni atoms ( $99 \pm 1$  at. %) while the second layer contains only  $30 \pm 5$  at. % Ni.<sup>26</sup>

The LEED model is further supported by core-level photoemission spectroscopy results by Barrett *et al.*<sup>10</sup> as well as LEIS measurements by Creemers and Deurinck.<sup>11</sup> At a temperature of 900–950 K the  $\text{Ne}^+$  and  $\text{He}^+$  signals show Pt concentrations of 98.8–99.7 at. % in the surface layer while iron is not detectable any more. This temperature is well below the order-disorder phase transition in the bulk. The strong Pt segregation is confirmed by calculations<sup>11</sup> on the thermodynamics of the segregation as well as by the segregation energy values given in the comprehensive compilations by Christensen *et al.*<sup>27</sup> and Ruban *et al.*,<sup>28</sup> reporting 0.63 and 0.37 eV/atom, respectively, for the exothermic dissolution of Fe in Pt bulk. In this context a similar investigation by Creemers on  $\text{Fe}_{99}\text{Pd}_1$  might be of interest, where the Pd concentration in the surface layer at about 900 K rises up to 55 at. %.<sup>29</sup>

#### A. The model

We shall now present our model as briefly discussed in the Introduction. It consists of a pure platinum layer on an ordered  $\text{Pt}_3\text{Fe}$  bulk, leading to Pt concentrations of 100 and 75 at. % in the top and underlying layers, respectively (see Fig. 1). In the real  $\text{Pt}_{80}\text{Fe}_{20}$  structure, some of the Fe atoms are randomly replaced by Pt which is neglected in our model. The model leads to two distinct surface Pt positions denoted by Pt1 and Pt2, respectively. While the former has a single subsurface Fe nearest neighbor the latter has only Pt neighbors. The influence of the iron atoms can therefore be expected to be lower on the Pt2 than on the Pt1 atoms. The

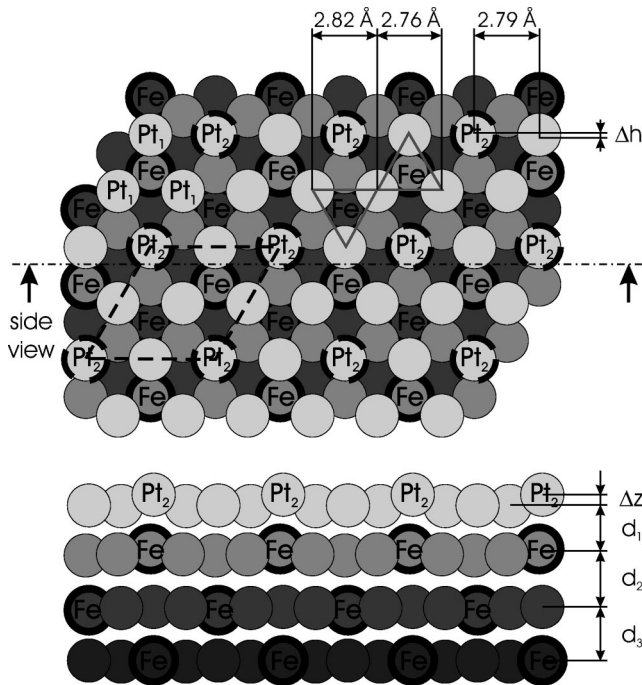


FIG. 1. Model of the Pt<sub>80</sub>Fe<sub>20</sub> (111) surface. The calculational supercell (equal to the surface unit cell) is indicated by the thick dashed line. The average bulk Pt<sub>3</sub>Fe bond length is 2.79 Å. Experimental and calculated values for the interlayer distances,  $\Delta h$ , and  $\Delta z$  are given in Table I below.

same model has been previously used by two of the authors in their extended Hückel investigations of the same surface.<sup>5</sup> In addition to this realistic model surface, we will also consider a fictitious bulk terminated surface, which keeps a Pt<sub>3</sub>Fe stoichiometry in the surface layer and will be labeled Pt<sub>3</sub>Fe (111).

### B. Magnetic configuration

The magnetic configuration of the Pt<sub>3</sub>Fe alloy, and consequently of alloys derived from it, is rather complicated because it is antiferromagnetic. The magnetic moment of the Fe atoms in Pt<sub>3</sub>Fe alloys has been calculated by Iwashita *et al.*<sup>30</sup> using a spin-polarized scalar-relativistic full-potential linear augmented plane-wave (FLAPW) method. Their value of about  $3.2\mu_B$  is in quite good agreement with our value of  $\mu_{Fe} = 3.28\mu_B$  in the Pt<sub>3</sub>Fe bulk. The magnetic moment on the Pt sites is negligible. The bulk shows two distinct antiferromagnetic configurations.<sup>31</sup> In the stoichiometric composition neighboring iron atoms (being second-nearest neighbors) have antiparallel spin (denoted as phase Q1). As the iron content is increased a second configuration consisting of planes of Fe atoms having parallel spin develops (named Q2). For the alloy catalyst, however, a more relevant result is the magnetic configuration of thin Pt<sub>3</sub>Fe films epitaxially grown on different oxide substrates.<sup>31</sup> The alloy remains antiferromagnetic but shows not only orientation- and stoichiometry-dependent but also substrate-dependent magnetic phases.

In our model we had to make some restrictions on the magnetic configuration to reduce the computational effort. A

four-layer surface slab in magnetic phase Q1 would require 64 atoms and is not feasible any more. We calculated the ferromagnetic and the layered antiferromagnetic Q2 phases for the model surface described above using an energy cutoff of only 300 eV, sufficient for clean surfaces. The magnetic moments of the iron atoms are  $\mu_{FM} = 3.30\mu_B$  and  $\mu_{AF} = \pm 3.35\mu_B$  respectively. Magnetic moments of Pt surface atoms are about  $0.15\mu_B$ , ferromagnetically coupled to the neighboring Fe atoms. Bulk Pt atoms have moments of  $\approx 0.3\mu_B$  and  $\approx 0$  for ferro- and antiferromagnetic Fe configurations, respectively. The antiferromagnetic slab indeed has a cohesive energy 17 meV/atom more stable than the ferromagnetic one. However, every surface Pt atom has only one magnetic (iron) nearest neighbor, hence the influence of the spins of neighboring iron atoms being antiparallel on the local electronic structure of Pt surface atoms is not significant. Since the focus of our study lies in the local chemical properties of the surface, we confined ourselves to adsorption on ferromagnetic slabs. Iron atoms in ferromagnetic Pt<sub>3</sub>Fe surfaces have magnetic moments of  $3.25\mu_B$ , both in the surface as well as in underlying layers.

### C. Surface relaxation

Initially all atoms in the surface slab are spaced with the bulk lattice constant of Pt<sub>3</sub>Fe in the respective magnetic configuration, which is 1.0%–2.8% smaller than the theoretical lattice constant of fcc Pt. Our calculational setup allowed for the top three layers to fully relax into the ionic ground state. We could then compare our results to the structure data obtained from LEED analysis.<sup>9</sup> The results are compiled in Table I, and the distances are indicated in Fig. 1. Explicitly given distances in Fig. 1 refer to the ferromagnetic slab as it is used throughout all further calculations.

All observed surface-reconstruction features can be traced back to the formation of very strong Pt-Fe bonds, shortened with respect to the average bulk distance. The strong bonds are a consequence of the significant *d*-band hybridization as discussed in the next section, and the shortening is eased through the reduced coordination at the surface. A similar contraction of heteroatomic bonds was also found in another early-late transition-metal surface alloy, namely, V/Pd (111).<sup>32,33</sup> In the surface layer this leads to triangles with a side length of only 2.76 Å above subsurface iron atoms compared to a bulk atomic distance of 2.79 Å in ferromagnetic Pt<sub>3</sub>Fe (see Fig. 1). In contrast the surface-atom separation above third-layer Fe atoms is increased to 2.82 Å. Lines of alternating inequivalent Pt surface atoms are slightly distorted in a zigzag fashion with a lateral displacement of  $\Delta h \approx 0.02$  Å in all magnetic configurations. Additionally the Pt2 atoms are pushed out of the surface by  $\Delta z \approx 0.1$  Å with respect to the Pt1 atoms.

Table I lists the interlayer distances, the distortion in the Pt1-Pt2 lines, and the buckling of the surface layer of pure Pt (111), Pt<sub>3</sub>Fe (111), and three magnetic configurations of Pt<sub>80</sub>Fe<sub>20</sub> (111), compared to the experimental data. The LEED fit used only a three-layer model, therefore the  $d_{34}$  value is missing. We observe that indeed the antiferromagnetic slab fits best with experimental values regarding the

TABLE I. Relaxation of the Pt, Pt<sub>3</sub>Fe, and Pt<sub>80</sub>Fe<sub>20</sub> (111) surfaces. The latter was calculated in nonmagnetic (NM), ferro- (FM), and Q2 antiferromagnetic (AF) configurations (see main text for details), the Pt<sub>3</sub>Fe surface in FM only.  $a$  is the bulk lattice constant, see Fig. 1 for the definition of geometric parameters. Interlayer distances in the cases where buckling of the layers occurs are weighted mean values. Experimental data is taken from Ref. 9.

	Pt		Pt <sub>3</sub> Fe		Pt <sub>80</sub> Fe <sub>20</sub>		Pt <sub>80</sub> Fe <sub>20</sub>		Pt <sub>80</sub> Fe <sub>20</sub>		LEED
	NM		FM		NM		FM		AF		
	[Å]	[%]	[Å]	[%]	[Å]	[%]	[Å]	[%]	[Å]	[%]	
$a$	3.99		3.95		3.88		3.95		3.92		3.90 Å
$d_{12}/\Delta d_{12}$	2.319	0.6	2.212	-2.9	2.314	3.3	2.301	0.9	2.301	1.7	1.2 %
$d_{23}/\Delta d_{23}$	2.281	-0.9	2.282	-0.1	2.198	-1.9	2.244	-1.6	2.258	-0.2	-0.6 %
$d_{34}/\Delta d_{34}$	2.314	0.4	2.231	-2.1	2.228	-0.5	2.242	-1.7	2.244	-0.8	
$\Delta z$			-0.08		0.09		0.11		0.12		0.09 Å
$\Delta h$			0.03		0.02		0.02		0.02		0.03 Å

interlayer distances, although our calculations are not in the expected Q1 but only in the simpler Q2 magnetic configuration. However, neither the ferromagnetic nor even the nonmagnetic model differ substantially in their ionic ground-state configuration, so from the point of surface geometry a ferromagnetic spin orientation introduces no serious errors.

Comparing the pure Pt and the alloy surfaces we note that the first two interlayer distances are shifted in the same direction, increased and decreased, respectively, although the effect is on average a little more pronounced in the alloy surface. The third- and fourth-layer separation, that differs in sign from the pure to the alloy surface, has to be taken with caution because in our model the atoms of the fourth layer are already kept fixed in their bulk position.

#### IV. ELECTRONIC STRUCTURE

The electronic structure of transition-metal alloy surfaces has only rarely been investigated in the past. However there exist both experimental as well as theoretical studies of bulk alloys with a significant  $d$ -band interaction between the constituents. Pick and Mikušik have applied a semiempirical tight-binding method to investigate the electronic structure of  $MTi$  and  $M_3Ti$  alloys with  $M$  being Ni, Pd, and Pt.<sup>34</sup> They compare the surface with the bulk electronic structure and report on the core-level shift of the surface atoms, however, they do not address the influence of Ti on the  $M$  surface atoms by comparing with the pure-metal surface. Results on the influence of an early transition metal (vanadium) on the electronic structure of a Pd (111) surface are presented in Ref. 33.

Photoelectron spectroscopy experiments on glassy Pd <sub>$x$</sub> Zr<sub>1- $x$</sub>  ( $25 \leq x \leq 35$ ) alloys have been performed and compiled by Oelhafen.<sup>35</sup> Among his findings is the shift of the Pd  $d$ -band center of mass towards higher binding energies by up to 2 eV, through the influence of the Zr measured using ultraviolet photoelectronic spectroscopy. The relatively small shifts in the core-level binding energies indicate a small charge transfer upon alloying.

The electronic structure of the Pt<sub>80</sub>Fe<sub>20</sub> alloy surface was also investigated both experimentally and theoretically before. Barrett *et al.*<sup>10</sup> report on core-level binding energies and

confirm the platinum segregation towards the surface by comparison of bulk and surface core-level energies. A work-function decrease of 0.2 eV from the pure Pt (111) to the alloy surface is reported in Ref. 8. From extended x-ray absorption fine-structure (EXAFS) measurements by Hlil *et al.*<sup>36</sup> it is known that there is an electron transfer from Fe to the Pt  $d$  band of about 0.1 electrons. Theoretical investigations applying the semiempirical extended Hückel calculation and neglecting spin polarization<sup>5</sup> preceded the present study.

In a first step we have determined the work function of Pt (111) and Pt<sub>80</sub>Fe<sub>20</sub> to be 5.79 and 5.55 eV, respectively, the difference being in good agreement with experiment. We have also calculated the charge transfer due to alloying by projecting the plane-wave expanded wave functions onto regions around the individual atoms. In both (the pure and the alloyed) surfaces the subsurface Pt atoms contain about 0.12-electrons more than the surface Pt atoms. The electron gain for Pt atoms due to neighboring Fe atoms is 0.065 and 0.075 electrons in the surface (Pt1) and subsurface layers, respectively, again in reasonable agreement with the experimental value, particularly with regard to the errors inevitably introduced by the projection procedure as well as in the EXAFS fit. Pt2 surface atoms, having no Fe nearest neighbor, experience only an electron transfer of 0.021 eV with respect to the pure surface. The third experimentally determined parameter, the core-level shift, is not yet accessible with our code.

Figure 2 shows the local densities of states (LDOS) of surface atoms. In Fig. 2 (a) the LDOS of a surface atom in pure Pt (111) are depicted. The  $d$ -band center of mass ( $d$ -COM) lies at 2.03 eV below  $E_F$ , the band is almost completely filled with its upper edge slightly above  $E_F$ , and the density of states at the Fermi level is  $n(E_F) = 1.78$  states/(eV atom). In the LDOS of a subsurface Fe atom of the alloy we can clearly see the importance of spin polarization [Fig. 2(b)]. While one spin band is completely filled [ $d$ -COM = -3.01 eV,  $n(E_F) = 0.06$  states/(eV atom)], the second spin component is close to empty with its center of mass almost at  $E_F$  and  $n(E_F) = 0.73$  states/(eV atom). In a nonmagnetic density-functional theory (DFT) calculation the

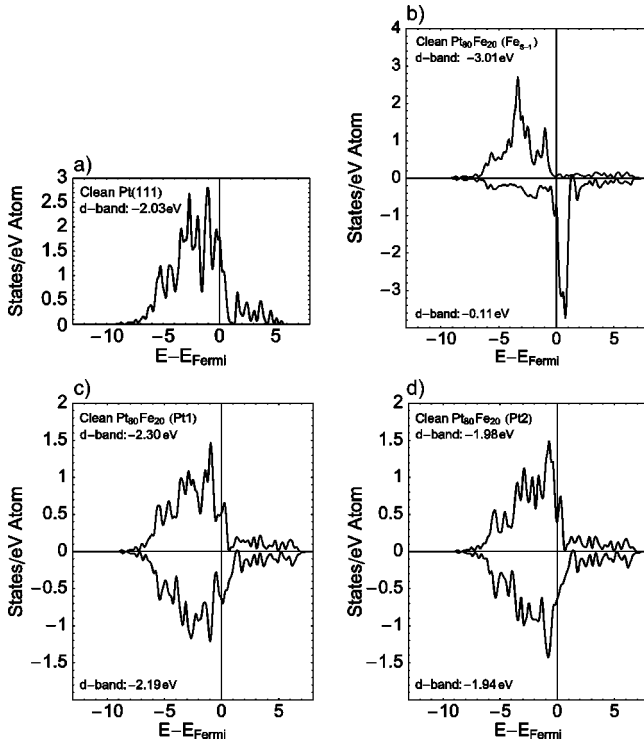


FIG. 2. Local densities of states (LDOS) for surface atoms in clean Pt (111) (a), the subsurface Fe atoms (b), and the two types of Pt surface atoms in Pt<sub>80</sub>Fe<sub>20</sub> (111) (c) and (d). The centers of mass of the  $d$  bands are indicated, relative to  $E_F$ , for both spin components.

Fermi level goes right through the peak of the Fe LDOS with a density of 4.94 states/(eV atom) at  $E_F$ , and considerable consequences for the electronic interaction with neighboring Pt atoms. Figures 2(c) and 2(d) show the LDOS of the two Pt surface species in our spin-polarized setup. Both  $d$  bands are shifted towards higher binding energies as a consequence of a strong hybridization of the  $d$  bands. We can observe the fast decrease of the iron atom's influence with distance by comparing the  $d$  bands of the Pt1 and Pt2 atoms. Such a decrease has previously been described also for V impurities in Pd (111) surfaces.<sup>33</sup> The  $d$ -COM for the Pt2 atom is close to the value for the pure Pt (111) surface, although  $n(E_F)$  is decreased with respect to the pure metal, to 0.40 and 0.64 states/(eV atom) for the spin-up and spin-down bands, respectively. For the surface Pt1 atoms  $n(E_F)$  is similar, namely, 0.52 and 0.64 states/(eV atom). The  $d$ -band shift is already visually clearly observable. It is stronger for the spin-up component ( $\Delta E = -0.27$  eV), because the majority bands of Fe and Pt are in the same energy range, but the value is still  $-0.16$  eV for the minority band where the Pt and Fe bands are more separated.

We can go even further and decompose the  $d$  bands of the Pt surface atoms into their orbital components as is shown in Fig. 3. The inset sketches the two surface atoms chosen and the orientation of the axes. We have plotted only the orbitals sticking out of the surface, since they favorably interact with adsorbates. The Pt2 orbitals show the expected rotational symmetry,  $d_{xz}$  and  $d_{yz}$ , are equal. For the Pt1 atom this

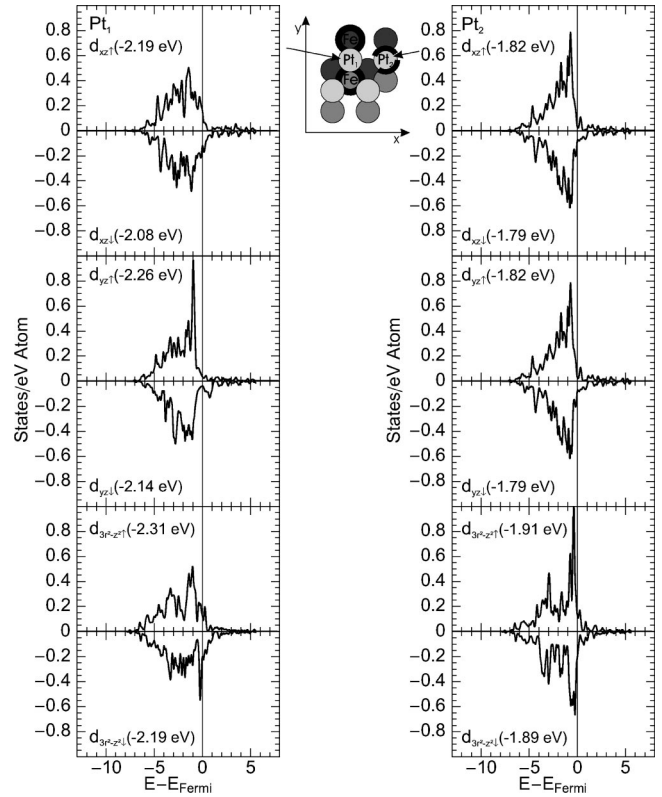


FIG. 3. Partial densities of states for Pt1 (left) and Pt2 (right) surface-atom  $d$  orbitals in Pt<sub>80</sub>Fe<sub>20</sub> (111). The numbers in the plots give the  $d$ -band center of mass for the corresponding orbital and spin components in eV relative to  $E_F$ . The drawing between the two panels shows the position of the respective surface atoms with respect to lower-lying atoms.

symmetry is broken. All orbitals exhibit a shift towards higher binding energies, but this shift is strongest for the  $d_{yz}$  and the  $d_{3z^2-r^2}$  orbitals, and here again for the spin component interacting with the Fe majority band. These are the orbitals pointing either directly towards the subsurface Fe atom ( $d_{yz}$ ) or towards the bond a subsurface iron atom forms with its neighbor ( $d_{3z^2-r^2}$ ). We can therefore expect adsorbates in high-symmetry positions forming bonds to these orbitals to be predominantly influenced in their adsorption energy relative to the pure Pt surface.

Coming back to the calculation for a fictitious nonmagnetic system, we observe an even stronger influence of the Fe atom on the electronic structure of the Pt atoms. Not only is the  $d$ -band of the Pt1 atoms more shifted than in the ferromagnetic case ( $\Delta E = -0.35$  eV), even for the Pt2 atoms the shift is still  $\Delta E = -0.2$  eV. Consequently adsorbates on the Pt2 species will “feel” much more the Fe atoms than in the spin-polarized calculation.

## V. ADSORPTION ENERGIES

We now turn our attention to adsorption energies of small species on the alloy surfaces and compare them to the pure-metal surface. Both test adsorbates, CO and H, have been extensively studied on Pt (111) surfaces (see references below) and there exist experimental values on the Pt<sub>80</sub>Fe<sub>20</sub> al-

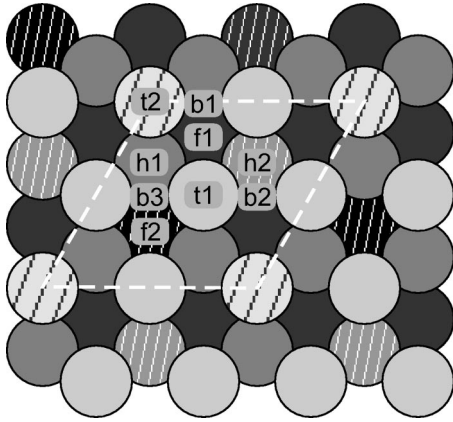


FIG. 4. High-symmetry adsorption positions on  $\text{Pt}_{80}\text{Fe}_{20}$  (111) surfaces. Dashed circles indicate the  $\text{Pt}_2$  atoms (surface layer) and Fe atoms (all other layers), respectively (cf. Fig. 1).

loy surface for CO (Ref. 7) as well as for H (Ref. 8).

Adsorption was only considered on high-symmetry positions. On the  $(2 \times 2)$  surface cell there are nine inequivalent high-symmetry adsorption sites, see Fig. 4. There are two top (t1, t2), two hcp hollow (h1, h2), and two fcc hollow (f1, f2) positions, each in a ratio 3:1 corresponding to the number of Pt1 and Pt2 atoms in the surface layer and the ratio of Pt and Fe atoms in deeper layers. Of the top positions t2 is further from the Fe atoms (on top Pt2), while for the hollows the index 2 denotes the position above an Fe atom. Additionally we locate three inequivalent bridge positions, b1 connecting the Pt2 atoms with neighboring Pt1, and b2 and b3 connecting two Pt1 atoms and located above second- and third-layer iron atoms, respectively.

The smallest possible surface cell of our model surface is a  $2 \times 2$  cell as indicated by the dashed line in Figs. 1 and 4. The initial (and lowest) coverage in our calculations is therefore  $\Theta = \frac{1}{4}$  monolayers. Higher coverages have been considered for H only.

### A. CO adsorption

The adsorption of CO on Pt (111) has been extensively studied experimentally (see, e.g., Ref. 37). CO adsorbs in an upright configuration on Pt with the carbon atom pointing downwards. For low coverages only the Pt top sites are occupied but already at a coverage of  $\Theta = 0.24$  a vibrational frequency associated with a bridge occupancy is observed in LEED experiments.<sup>37</sup> At  $\Theta = 0.5$  a well-ordered  $c(4 \times 2)$ -2CO structure develops with an equal number of CO molecules on top and bridge sites. The metal-carbon bond lengths have been determined by LEED (Ref. 38) to be 1.85 and 2.08 Å for top and bridge sites, respectively, with a C-O bond length of 1.15 Å in both cases. There are also numerous theoretical studies on that issue, see, e.g., Ref. 39, and references therein.

Other recent theoretical investigations of CO adsorption on alloy surfaces that are of interest in the present context are the following: Gauthier *et al.*<sup>40</sup> have studied Pt-Co surface alloys, both experimentally by scanning-tunneling microscopy and theoretically using DFT calculations. They observe

TABLE II. CO on Pt and  $\text{Pt}_{80}\text{Fe}_{20}$ : Adsorption energies, adsorption energy differences between pure Pt and alloy surfaces ( $\Delta E_{\text{ad}}$ ), geometries of the adsorbed molecules, and harmonic C-O stretching frequencies for CO adsorption on high-symmetry positions.

Pt (111)						
Position	$E_{\text{ad}}$ [eV]	$d_{\text{CO}}$ [Å]	$z(\text{C})$ [Å]	Tilt angle [°]	$\omega_h$ [ $\text{cm}^{-1}$ ]	
Top	1.585	1.158	1.849	0.0	2064	
Bridge	1.723	1.178	1.442	0.4	1870	
fch	1.747	1.192	1.323	0.0	1773	
hch	1.739	1.193	1.333	0.0	1776	
$\text{Pt}_{80}\text{Fe}_{20}$ (111)						
Position	$E_{\text{ad}}$ [eV]	$\Delta E_{\text{ad}}$ [eV]	$d_{\text{CO}}$ [Å]	$z(\text{C})$ [Å]	Tilt angle [°]	$\omega_h$ [ $\text{cm}^{-1}$ ]
t1	1.284	-0.301	1.157	1.861	1.2	2066
t2	1.413	-0.172	1.158	1.843	0.0	2066
b1	1.486	-0.237	1.181	1.465	2.2	1892
b2	1.183	-0.540	1.181	1.450	1.5	1890
b3	1.340	-0.383	1.181	1.472	1.2	1885
f1	1.498	-0.248	1.192	1.374	2.9	1811
f2	1.065	-0.682	1.189	1.335	0.0	1824
h1	1.449	-0.290	1.192	1.336	5.1	1817
h2	1.306	-0.433	1.191	1.355	0.0	1823

a large influence of strain effects because of the -4.6% lattice mismatch of the alloy with respect to the pure Pt (111) surface. For  $\text{Pt}_3\text{Fe}$  the lattice mismatch is only -1.1%, and strain effects are therefore small compared to electronic effects for a Pt covered surface. Furthermore, two of us (Hirschl and Hafner) have studied the adsorption of CO on V/Pd (111) surface alloys,<sup>41</sup> observing similar features as described below in good agreement with experimental results.<sup>42</sup> Delbecq and Sautet have theoretically investigated CO on  $\text{Pd}_3\text{Mn}$  (100),<sup>43</sup> where the most stable site changes from hollow to top through the influence of the Mn atoms.

CO adsorption energies for pure Pt and Pt-Fe alloy surfaces as well as some geometrical data for a coverage  $\Theta = \frac{1}{4}$  are compiled in Table II. We note that on pure Pt (111) the face-centered hollow (fch) site is theoretically the energetically most favored adsorption site in contradiction with experiment. This well-known shortcoming of DFT (Ref. 39) probably arises from the underestimation of the HOMO-LUMO (highest occupied molecular orbital-lowest unoccupied molecular orbital) gap of the CO molecule characteristic for DFT calculations. The question has been addressed recently using the B3LYP functional which combines the Becke exchange and the Lee-Yang-Parr correlation functional with Hartree-Fock exchange.<sup>44</sup> The theoretical carbon-metal bond lengths for on-top and bridge adsorption, being 1.85 and 2.02 Å, respectively, are in excellent agreement with the experimental values (1.85 and 2.08 Å, Ref. 38). This proves that despite the prediction of the wrong adsorption site, DFT yields reasonable results for CO adsorption on Pt regarding its geometric features.

The adsorption energies on the alloy surface are considerably decreased with respect to the pure Pt (111) surface.

TABLE III. H on Pt and Pt<sub>80</sub>Fe<sub>20</sub>: Adsorption energies ( $E_{\text{ad}}$ ), adsorption energy differences ( $\Delta E_{\text{ad}}$ ) between pure Pt and alloy surfaces, height of the adsorbate above the surface, harmonic-vibrational frequencies, vibrational zero-point (ZP) energy, and total adsorption energy for high-symmetry adsorption positions on Pt (111) and Pt<sub>80</sub>Fe<sub>20</sub> (111).

Pt (111)								
Position	$E_{\text{ad}}$ [eV]	$h$ [Å]	$\omega_h$ [cm <sup>-1</sup> ]			$E_{\text{zp}}$ [eV]	$E_{\text{ad,tot}}$ [eV]	
Top	0.438	1.561						
Bridge	0.449	1.020						
fch	0.499	0.821	1056	864	571	0.153	0.346	
hch	0.459	0.829						
Pt <sub>80</sub> Fe <sub>20</sub> (111)								
Position	$E_{\text{ad}}$ [eV]	$\Delta E_{\text{ad}}$ [eV]	$h_H$ [Å]	$\omega_h$ [cm <sup>-1</sup> ]			$E_{\text{zp}}$ [eV]	$E_{\text{ad,tot}}$ [eV]
t1	0.201	-0.238	1.567					
t2	0.461	0.023	1.560	2275	456	450	0.197	0.264
b1	0.359	-0.090	1.050	1393	936	309	0.164	0.195
b2	0.255	-0.194	1.079					
b3	0.255	-0.194	1.080					
f1	0.376	-0.123	0.925	1154	714	605	0.153	0.223
f2	0.200	-0.299	0.823	1034				
h1	0.330	-0.129	0.896	1126				
h2	0.242	-0.217	0.932	1138				

The second column in the lower part of Table II gives the adsorption energy difference on alloy and pure-metal surfaces. The further away the adsorption site from a subsurface iron atom, the closer the adsorption energy to the pure-metal value. The smallest decrease is observed for the t2 on-top adsorption site. The comparatively too low adsorption energy on top sites with respect to hollow adsorption persists on the alloy, and experimentally the favored adsorption positions are on top. The largest influence of iron is found on the f2 site. The  $d$  orbitals of the neighboring Pt1 atoms interacting with the adsorbate are affected by the second-layer Fe atoms. A second strongly influenced site is h2: the immediately underlying Fe atom is closer here and again the  $d$  orbitals of the surface atoms pointing towards the adsorbates are those which experience the largest shift due to alloying. We might mention at this point that the energetical ordering of the two top adsorption sites is reversed in nonmagnetic DFT calculations in agreement with the semiempirical nonmagnetic investigations in Ref. 5.

Whereas large differences in the adsorption energies are found between the inequivalent top, bridge, and hollow sites (the difference between f1 and f2 being as large as 0.43 eV), the C-O bond length, the adsorption height, and the C-O stretching frequency depend only on the site symmetry and show no correlation with the adsorption energy. In the sequence  $t \rightarrow b \rightarrow h$ , the adsorption heights and the stretching frequencies decrease, while the C-O bond lengths increase. Different top, bridge, or hollow positions however cannot be resolved by measurements of the stretching frequency. Still, the stretching frequencies are, especially for the hollow adsorption sites, significantly increased (by up to 50 cm<sup>-1</sup>)

with respect to the pure-metal surface (see Table II). The tilting of the C-O molecule by up to 5° with respect to the surface normal is a purely electronic effect through the stronger bonding of the adsorbate (via the C atom) to the Pt2 surface atom. The oxygen atom is canted away from Pt2 in all cases.

The reduction in the adsorption energy can be straightforwardly explained by the influence of the Fe atoms on the surface Pt  $d$ -band orbitals. The more the surface  $d$ -band orbitals interacting with the adsorbate are affected by Fe, the lower the adsorption energy. A more detailed discussion of the electronic adsorbate-surface interaction is presented in Sec. VI.

### B. H adsorption

The adsorption of hydrogen on Pt (111) is also well documented. Graham *et al.*<sup>45</sup> have determined the diffusion barrier of atomic H on Pt (111) at low coverages via quasielastic helium atom scattering measurements to be  $68 \pm 5$  meV. DFT calculations for H on Pt (111) have been performed among others by Nobuhara *et al.*<sup>46</sup> The authors present potential-energy curves for H adsorption over various metals. From their calculations, H on Pt (111) has the lowest diffusion barrier. Olsen *et al.* included scalar-relativistic effects in their calculations.<sup>47</sup> However, they get the wrong preferred adsorption site for gradient-corrected functionals and a considerable overbinding for plain local-density approximation (LDA). Similar adsorption energies as on Pt (111) have been reported for the hollow and bridge sites of Pd (111) by Dong *et al.*,<sup>48</sup> although on the Pd surface on-top adsorption is unstable.

Adsorption energies and heights of atomic hydrogen on Pt (111) and  $\text{Pt}_{80}\text{Fe}_{20}$  (111) are compiled in Table III for the coverage  $\Theta = \frac{1}{4}$ . On the pure surface the fcc hollow is the most stable adsorption position, in agreement with experiment. The energy difference to bridge adsorption is only 50 meV, to top 60 meV. This fits the measured low diffusion barrier of H on Pt (111). On the alloy surface the adsorption energies are again, in general, decreased, and the energetical ordering of the different high-symmetry positions is quite similar to the CO adsorption, with one important difference: On-top Pt2 adsorption is even slightly more stable on the alloy than on-top adsorption on the pure surface. In combination with the tiny energy differences of the different adsorption sites on the pure surface, this makes the Pt2 top site the most stable adsorption position for hydrogen on  $\text{Pt}_{80}\text{Fe}_{20}$  (111).

The energy difference to the f1 position is only 85 meV, making a consideration of the zero-point energy of the adsorbate indispensable. Results are also recorded in Table III. We calculated the three vibrational frequencies of the adsorbate, neglecting coupling to the surface atoms (a reasonable approach considering the large mass difference). The frequency for vibrations of the atom normal to the surface is by far highest for on-top adsorption, but, in contrast, the potential surface is particularly flat there, leading to low frequencies for frustrated translations parallel to the surface. After zero-point corrections the Pt2 top position remains the most stable by 40 meV for this low coverage. To our knowledge this is the first time that on-top hydrogen adsorption turned out to be energetically favored on a flat transition-metal surface.

Adsorption heights do not correlate to adsorption energies but rather to the coordination of the adsorbate. The smaller differences between sites with equal coordination are related to the local geometry of the surface around the adsorption position. Where the Pt-Pt distance in the surface is smaller, the H atom is adsorbed higher from the surface.

Since there is only one t2 adsorption site per  $2 \times 2$  cell, on-top adsorption is only favored for very low coverages. The adsorption energy per unit cell versus the coverage is plotted in Fig. 5 for top and fch adsorption. The largest positive value corresponds to the most stable situation. The dashed lines show the sum of low-coverage adsorption energies, i.e., a situation without interaction of vicinal adsorbates. Full lines show the calculated adsorption energies. Although for fch adsorption the interadsorbate repulsion and the poisoning through adsorbates on neighboring sites is larger than for top adsorption, hollow adsorption becomes favored already at a half-monolayer coverage because of the low adsorption energy on the t1 site. An experimental verification of the top adsorption through vibration frequency measurements, therefore, has to be performed at very low H coverages.

### C. Influence of Fe surface atoms

The fact that subsurface iron atoms reduce the adsorption strength of both CO and H, resulting in preferred adsorption sites far away from the Fe atoms, seems to contradict results

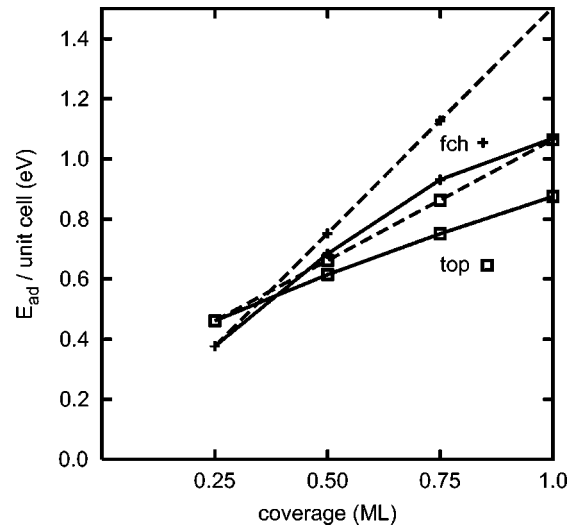


FIG. 5. Coverage dependence of the H adsorption energy per  $2 \times 2$  unit cell on top and fch sites. The dashed lines give the values if vicinal adsorbates had no influence on each other (see main text for details).

from pure Fe surfaces. Eder *et al.* have calculated the adsorption of H on  $\alpha$ -Fe (110) and get adsorption energies of 0.69 eV in the hollow sites,<sup>49</sup> almost 40% more than the 0.5 eV adsorption energy on pure Pt. Experimental results on Fe (111) surfaces confirm this strong affinity of Fe for H.<sup>50</sup> CO adsorption on  $\alpha$ -Fe (110) and (100) has been studied by Stibor *et al.*<sup>51,52</sup> Adsorption energies range around 2 eV for a coverage of  $\Theta = \frac{1}{4}$  and the CO molecule is tilted on Fe (100) by up to  $50^\circ$  with respect to the surface normal. The tilting also leads to a strong reduction of the activation energy for CO dissociation. Spiřák and Hafner have investigated CO chemisorption on thin  $\gamma$ -Fe films on Cu (100).<sup>53</sup> They observed a significant very localized demagnetization (up to  $1.42 \mu_B$ ) of surface Fe atoms upon a direct interaction with the adsorbate.

We have investigated how our test adsorbates react to the existence of iron atoms in the surface through a bulk termi-

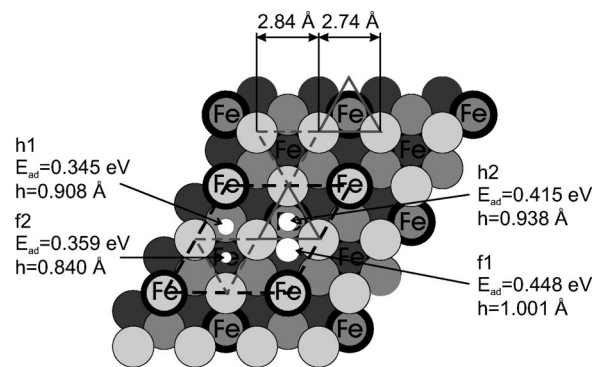


FIG. 6. Surface relaxation of bulk terminated  $\text{Pt}_3\text{Fe}$  (111) surfaces (having Fe atoms in the surface layer) and adsorption geometries of hydrogen atoms in different high-symmetry positions. Adsorbates neighboring surface Fe atoms are pushed off center away from Fe. The diameter of the H atoms (white disks) is proportional to the height of the atoms above the surface.

TABLE IV. H and CO on Pt<sub>3</sub>Fe: Adsorption energies, adsorption geometries, and adsorption energy differences between pure Pt (111), and Pt<sub>3</sub>Fe, the bulk terminated structure having Fe atoms in the surface. Additionally the magnetic moment of the surface Fe atom is given [ $\mu_{\text{Fe}(\text{clean})} = 3.25\mu_B$ ]. CO tilting angles are given with respect to the surface normal with the O atom canted towards the surface iron.

Pt <sub>3</sub> Fe (111)							
Adsorbate	Position	$E_{\text{ad}}$ [eV]	$\Delta E_{\text{ad}}$ [eV]	$d_{\text{CO}}$ [Å]	$z(\text{ads})$ [Å]	Tilt angle [°]	$\mu_{\text{Fe}(\text{surf})}$ [ $\mu_B$ ]
H	t1	0.321	-0.075		1.578		3.264
	t2 (top Fe)	-0.363	-0.801		1.535		2.747
	f1	0.448	-0.051		1.001		3.241
	f2	0.359	-0.140		0.840		3.277
	h1	0.345	-0.114		0.908		3.202
	h2	0.415	-0.044		0.938		3.290
CO	t1	1.509	-0.076	1.158	1.871	2.5	3.274
	t2 (top Fe)	1.206	-0.379	1.164	1.773	0.0	1.914
	f1	1.598	-0.149	1.184	1.515	14.5	3.227
	f2	1.352	-0.395	1.192	1.329	0.0	3.284
	h1	1.306	-0.433	1.193	1.322	2.1	2.943
	h2	1.652	-0.087	1.192	1.393	0.0	3.296

nated Pt<sub>3</sub>Fe (111) model surface (see Fig. 6). This fictitious model does not take into account the strong segregation of Pt at the surface, nevertheless the LEED model of the Pt<sub>80</sub>Fe<sub>20</sub> alloy allows for a few percent of Fe atoms in the surface layer.

Adsorption energies and geometries as well as the magnetic moment of the surface iron atom are compiled in Table IV. Iron atoms in a Pt<sub>3</sub>Fe (111) alloy surface definitely have a negative effect on the adsorption energy with respect to the pure-metal Pt surface. Particularly the iron on-top adsorption is unfavorable, partly because it is associated with a large demagnetization of the surface iron atom. Its value of  $1.3\mu_B$  is very similar to the value for CO chemisorption on thin  $\gamma$ -Fe films ( $1.42\mu_B$ ).<sup>53</sup> For all other adsorption positions the loss of magnetic moment of the surface iron is not more than 10% from its clean surface value of  $3.25\mu_B$ . The preference for nonmagnetic surface atoms can be compared to the adsorption of CO on Pd<sub>3</sub>Mn, where the adsorbate preferably adsorbs on top of the nonmagnetic Pd atoms.<sup>43</sup> In spite of this adverse effect of iron in the surface, several high-symmetry positions exhibit a higher adsorption energy than on the Pt<sub>80</sub>Fe<sub>20</sub> surface for both adsorbed species, e.g., t1 and h2. While for H adsorption all hollow sites are preferred with respect to on-top adsorption, in the case of CO as adsorbate the t1 position is already the third-most favorable position. Experimentally the t1 adsorption position is likely to be the most favorable one following the discrimination of CO on-top adsorption in DFT calculations on pure Pt surfaces as discussed above. Comparing the different hollow adsorption sites, the trends are equal for both adsorbates, with f1 and h2 lying energetically well below f2 and h1. This will be first discussed for the case of atomic H adsorption, while the CO adsorption, with the additional feature of molecular tilt, will be treated afterwards.

The link between iron-influenced Pt  $d$ -band orbitals and ad-

sorption energy cannot as readily be established as can in the case of the Pt-terminated alloy. An effect that can influence adsorbate-surface interactions besides the electronic interaction with neighboring atoms is the strain in the surface. The impact of strain on hydrogen adsorption on transition-metal surfaces is discussed in Ref. 54. As atomic distances are decreased, the  $d$  band broadens and its center of mass is shifted down in energy to keep the  $d$  band filling constant, which reduces adsorption energies. In the Pt<sub>3</sub>Fe surface the Pt-Pt distances are not uniformly strained. Figure 6 depicts the surface and the hydrogen adsorption positions in hollow sites, the diameter of the H atom being related to its height above the surface. We note that H atoms in hollows next to Fe surface atoms are adsorbed off center, being repulsed from the Fe atom. As a consequence of the Pt-Fe bond shortening as described above in the context of Pt<sub>80</sub>Fe<sub>20</sub>, two types of equilateral Pt<sub>3</sub> triangles form in the surface, one above a subsurface Fe atom with decreased side length compared to the bulk distance of  $2.79 \text{ \AA}$  (solid lines in Fig. 6), and one above a third-layer Fe atom with increased distance (dashed lines). Areas of tensile strain alternate with areas of compressive strain. We can now apply the concept of strain-induced electronic-structure changes to individual orbitals in the direction of shortened or lengthened bonds within the surface. The opposite ends of these orbitals point out of the surface and can interact with adsorbates. As can be inferred from the figure, the hydrogen interacting with  $d$  orbitals shifted towards higher binding energies because of decreased atomic distances (on the h1 site) is least bound, while the adsorbate on site f1, interacting with  $d$  orbitals closer to the Fermi energy, is the most strongly bound. Also the height of the adsorbed atoms can be explained by the local geometry of the surface. In the vicinity of shortened bonds the adsorbates are pushed out of the surface whereas they approach the surface closer near longer bonds. Additionally we can

observe the repelling effect of the surface iron atom pushing neighboring adsorbates towards the next bridge site.

The situation is very similar for adsorbed CO molecules, though there are additional internal geometry parameters of the adsorbate. The C-O distances again do not correlate to the adsorption energies but only to the coordination of the adsorption site. The comparatively short C-O bond length for adsorption at the f1 site is explained by the shift of the adsorbate towards the bridge position. While on the Pt-terminated surface the tilt is initiated by a favored interaction (and thereby attraction) of the carbon atom towards the Pt2 atom, on the Pt<sub>3</sub>Fe surface it is an electronic repulsion from the Fe atom. However, on the Pt<sub>3</sub>Fe surface the tilt is much more pronounced than on Pt<sub>80</sub>Fe<sub>20</sub>, due to an additional effect. In the case of Fe surface atoms the first effect cants the O atoms towards the Fe atom. The *p* orbitals of the O atom normal to the molecular axis (contributing to the molecular 1  $\pi$  and 2  $\pi^*$  orbitals) bond with the iron *d* orbitals pointing towards them. The resulting bonding interaction between O and Fe further tilts the CO molecule. This is most apparent at the f1 adsorption site with a tilt angle of 14.5°. On pure Fe (100) a tilt angle of more than 50° for CO was calculated by Stibor *et al.*,<sup>51</sup> leading to an energy gain of almost 0.5 eV with respect to the molecule adsorbed in an upright configuration.

## VI. DISCUSSION

In the previous sections we have found that both test adsorbates, CO and atomic hydrogen, adsorb weaker on iron-modified Pt (111) surfaces than on pure Pt (111), no matter if the surface layer is pure Pt or Pt<sub>3</sub>Fe. Figure 7 depicts the results for the Pt<sub>80</sub>Fe<sub>20</sub> surface by visualizing the adsorption energy differences between pure and alloyed surfaces. The panels for CO (top) and hydrogen (bottom) look very similar. Near the surface atoms of type Pt2 the adsorption energies approach the values for the pure Pt surface. The reduction is strongest above a third-layer Fe atom. All three surface Pt atoms interact with different second-layer Fe atoms, hence the two effects of downshifted Pt *d*-band orbitals and direct interaction of the adsorbate with Fe atoms are combined most efficiently.

CO adsorption on the two Pt top sites of the Pt covered Pt<sub>80</sub>Fe<sub>20</sub> surface will now serve as an example for the analysis of the adsorption energy differences in terms of electronic-structure changes. Figure 8 shows the changes of the spin-polarized electronic DOS upon adsorption on the two sites. The dashed lines are the clean surface-atom densities of state, the full lines the DOS after CO adsorption. The dashed regions indicate the depleted bands through adsorption either by donation to the 2  $\pi^*$  molecular orbital or by a downshift of the band. The differences in the *d*-band centers of the two surface Pt atoms are less than 0.15 eV after adsorption, compared to more than 0.3 eV for the spin-up *d* band on the clean surface. The electronic interaction of the adsorbate with the surface has two main contributions. On one hand the lone pair of the CO 5  $\sigma$  orbital (the HOMO) has a destabilizing four-electron interaction with the almost full  $d_{3z^2-r^2}$  orbital of the metal. On the pure-metal

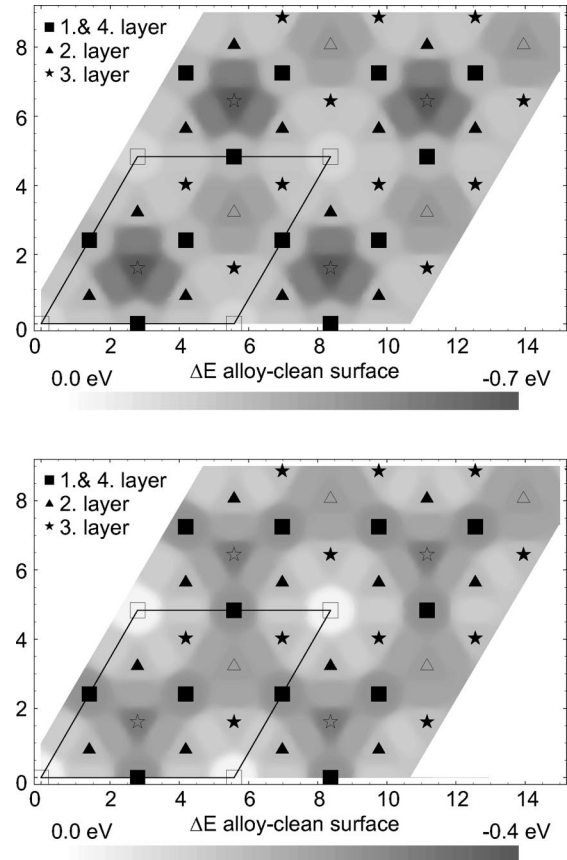


FIG. 7. Adsorption energy differences of CO (top) and H (bottom) adsorption on Pt<sub>80</sub>Fe<sub>20</sub> (111) surfaces compared to the pure Pt (111) surface. Open symbols indicate Pt2 (surface layer) and Fe atoms (other layers), respectively.

surface and above the Pt2 atom on the alloy surface this effect is, however, not very strong, because the antibonding contribution is pushed above  $E_F$  easily, and hence is vacant. In the case of a lower position of the *d* band as in the Pt1 atoms, more antibonding states are filled and the adsorbate is less stable. The second interaction is the back donation between occupied *d* orbitals and the empty 2  $\pi^*$  orbital of CO. Lowering the Pt *d* band increases the energy separation of the orbitals and weakens the chemisorption. This explains the larger adsorption-induced *d*-band shift for adsorption of on-top Pt2 which initially shows a higher *d* band.

Besides this adverse effect of the Pt *d* band downshift due to bond formation with neighboring Fe atoms on the interaction of the surface with the HOMO as well as the LUMO of the adsorbate, we could identify two more reasons for an adsorption energy decrease. First there is an influence of strain on the surface-atom orbitals, that is more pronounced in Pt<sub>3</sub>Fe surfaces than in Pt-terminated alloy surfaces where the bond-length differences are smaller. The *d*-orbital bond efficiency towards adsorbates increases for stretched metallic bonds. The second effect, arising only in the case of Fe atoms in the surface, comes directly from the electronic structure of a (more or less) isolated iron atom in a close-packed Pt surface. Having a nearly completely filled majority-spin

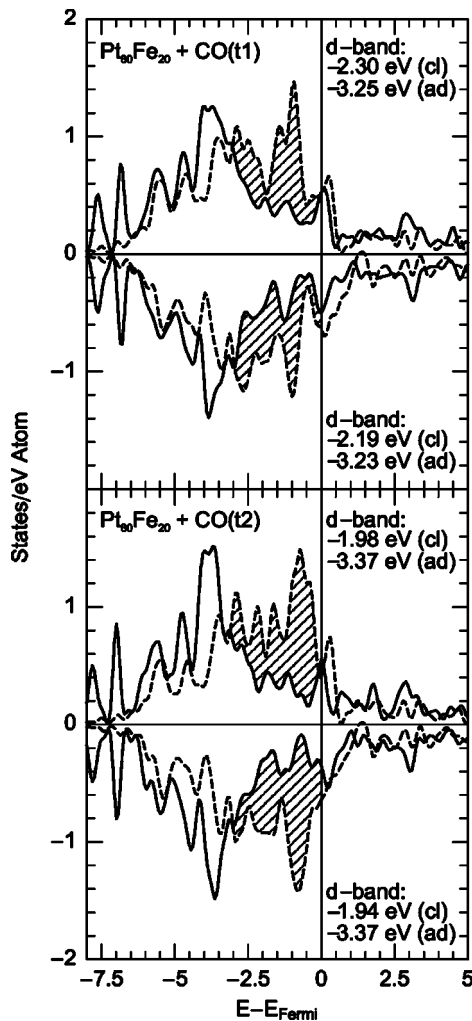


FIG. 8. Local density of states of the surface Pt atoms for CO adsorbed on top of Pt1 and Pt2. Dashed lines are the DOS of the respective atoms of the clean surface, and the dashed regions are the electronic bands depleted through adsorption. Adsorption of on-top Pt2 is 130 meV more stable.

band well below  $E_F$ , and an almost empty minority band with also no considerable density of states at the Fermi energy, it is unfavorable for the adsorption of carbon and hydrogen.

Our results on the Pt<sub>80</sub>Fe<sub>20</sub> (111) surface can be compared to experimental findings. For CO, temperature programmed desorption (TPD) measurements have shown two distinct desorption peaks.<sup>7</sup> The high-temperature peak is very close to the CO desorption from pure Pt (111), and the low-temperature peak indicates a second adsorption site with an adsorption energy about 100 meV lower. Though the theoretically determined absolute adsorption energies do not match the experimental results (see also Ref. 33), the theoretical adsorption energy difference of 130 meV between the two top adsorption sites is in excellent agreement with experiment, confirming the two top positions as the populated sites at low coverages. Also C-O vibrational frequencies determined by electron-energy-loss spectroscopy (EELS) mea-

surements of 2100 and 1850 cm<sup>-1</sup> for on-top and bridge adsorptions respectively, are reasonably well reproduced by DFT calculations.

Concerning hydrogen adsorption experiments on Pt<sub>80</sub>Fe<sub>20</sub> surfaces, only adsorption energies from TPD measurements are reported.<sup>8</sup> Two desorption peaks, separated by 85 meV, can be observed. The high-temperature (HT) peak is slightly above the desorption peak on pure Pt (111). While the area under the low-temperature (LT) peak increases with larger hydrogen exposure, the integral over the HT peak levels up already below an exposure of 10 L. We identify the LT and HT peaks with adsorption in fcc hollows, dominating for higher coverage, and on-top Pt2, the most favorable adsorption position for low coverages. High resolution EELS investigations at low coverages might in the future verify our finding of a stable on-top adsorption through its distinct hydrogen vibration frequency normal to the surface, well above the one on other adsorption sites.

## VII. CONCLUSIONS

We can summarize that, although the surface of the Pt<sub>80</sub>Fe<sub>20</sub> alloy is a pure Pt layer, it behaves in a very different manner compared to a pure-metal Pt surface. Subsurface iron reduces adsorption energies of CO and H on Pt (111) much as subsurface V atoms do on Pd (111).<sup>41</sup> Preferred adsorption sites are related to surface atoms with a minimum number of Fe neighbors in the subsurface layer. A strong Pt-Fe interaction shifts the Pt *d* bands down in energy and the Pt atoms in the alloy surface are more negatively charged than Pt atoms in a pure-metal surface. The resulting competition of the electron donating interactions of Fe and adsorbates such as CO or H is one reason for the reduced adsorption energies. The other reason is the increased energy distance of surface *d*-band and adsorbate molecular orbitals due to the *d*-band shift, reducing interaction abilities. Fe atoms in the alloy carry a magnetic moment almost as large as in the free atom. A spin-polarized treatment of the alloy surface is essential to describe the Fe-Pt interaction correctly. Although the surface Pt atoms carry no significant magnetic moment, neglecting spin polarization changes the results qualitatively (see Sec. V A).

Iron atoms in the surface do not further reduce adsorption energies. However, they change the local surface geometry and provoke strain-induced electronic-structure changes that in turn affect the local chemical reactivity. Both adsorbates avoid the vicinity of surface iron atoms, but an additional effect is observed in the case of CO adsorption, namely, a very pronounced tilting of the adsorbate with the oxygen atom canted towards the iron. This deviation of the molecular axis from the surface normal was already noticed on pure  $\alpha$ -Fe surfaces to increase the adsorption energy remarkably and indicates a favorable Fe-O interaction.

The present study is a first step towards the understanding of the increased selectivity of modified Pt surfaces for the hydrogenation of unsaturated aldehydes to unsaturated alcohols, i.e., the hydrogenation of the C=O double bond instead of the C=C double bond. The latter is preferably hydroge-

nated over pure Pt (111). We have now mapped the potential-energy surface above the alloy surface for small adsorbates and have identified the effects that are responsible for the decreased reactivity of the alloy. Not only might the weaker adsorption energy play an important role in the modified reactivity of the alloy compared to the pure surface, also the affinity of surface Fe atoms to oxygen atoms deserves further attention. With this knowledge we can now proceed to investigate the adsorption of simple unsaturated aldehydes and their effect on the local surface properties.

## ACKNOWLEDGMENTS

We gratefully acknowledge financial support by the European Commission's Human Potential Program (Marie Curie Training Site Grant No. MCFH-1999-01219) and the Austrian Fonds zur Förderung der Wissenschaftlichen Forschung within the Science College "Computational Materials Science" (Grant No. FWF-WK004). Furthermore we thank the CINES and IDRIS (Project No. 609) in Montpellier and Orsay, respectively, for generous provision of CPU time.

\*Electronic address: robin.hirschl@univie.ac.at

- <sup>1</sup>P. Beccat, J.C. Bertolini, Y. Gauthier, J. Massardier, and P. Ruiz, *J. Catal.* **126**, 451 (1990).
- <sup>2</sup>M. English, V.S. Ranade, and J.A. Lercher, *Mol. Catal. A: Chem.* **121**, 69 (1997).
- <sup>3</sup>T.B.L.W. Marinelli, S. Nabuurs, and V. Ponc, *J. Catal.* **151**, 431 (1995).
- <sup>4</sup>V. Ponc, *Appl. Catal., A* **149**, 27 (1997).
- <sup>5</sup>F. Delbecq and P. Sautet, *J. Catal.* **164**, 152 (1996).
- <sup>6</sup>G.A. Somorjai, *Introduction to Surface Chemistry and Catalysis* (Wiley, New York, 1994).
- <sup>7</sup>A. Atli, M. Abon, P. Beccat, J.C. Bertolini, and B. Tardy, *Surf. Sci.* **302**, 121 (1994).
- <sup>8</sup>A. Atli, M. Almot, J.J. Ehrhardt, J.C. Bertolini, and M. Abon, *Surf. Sci.* **269**, 365 (1992).
- <sup>9</sup>P. Beccat, Y. Gauthier, R. Baudoing-Savois, and J.C. Bertolini, *Surf. Sci.* **238**, 105 (1990).
- <sup>10</sup>N. Barrett, C. Guillot, J.C. Bertolini, J. Massardier, and B.C. Khanra, *Surf. Sci. Lett.* **260**, L11 (1992).
- <sup>11</sup>C. Creemers and P. Deurinck, *Surf. Interface Anal.* **25**, 177 (1997).
- <sup>12</sup>W. Kohn and L.J. Sham, *Phys. Rev.* **140**, A1133 (1965).
- <sup>13</sup>U. von Barth and L. Hedin, *J. Phys. C* **5**, 2064 (1972).
- <sup>14</sup>F. Delbecq and P. Sautet, *J. Catal.* **211**, 398 (2002).
- <sup>15</sup>G. Kresse and J. Furthmüller, *Phys. Rev. B* **54**, 11 169 (1996).
- <sup>16</sup>G. Kresse and J. Hafner, *Phys. Rev. B* **49**, 14 251 (1994).
- <sup>17</sup>G. Kresse and J. Hafner, *Phys. Rev. B* **47**, 558 (1993).
- <sup>18</sup>G. Kresse and J. Furthmüller, *Comput. Mater. Sci.* **6**, 15 (1996).
- <sup>19</sup>D.M. Wood and A. Zunger, *J. Phys. A* **18**, 1343 (1985).
- <sup>20</sup>J.P. Perdew and Y. Wang, *Phys. Rev. B* **45**, 13 244 (1992).
- <sup>21</sup>H.J. Monkhorst and J.D. Pack, *Phys. Rev. B* **13**, 5188 (1976).
- <sup>22</sup>P.E. Blöchl, *Phys. Rev. B* **50**, 17 953 (1994).
- <sup>23</sup>G. Kresse and D. Joubert, *Phys. Rev. B* **59**, 1758 (1999).
- <sup>24</sup>R.P. Feynman, *Phys. Rev.* **56**, 340 (1939).
- <sup>25</sup>D. Loffreda, D. Simon, and P. Sautet, *Surf. Sci.* **425**, 68 (1999).
- <sup>26</sup>Y. Gauthier, Y. Joly, R. Baudoing, and J. Rundgren, *Phys. Rev. B* **31**, 6216 (1985).
- <sup>27</sup>A. Christensen, A.V. Ruban, P. Stoltze, K.W. Jacobsen, H.L. Skriver, J.K. Nørskov, and F. Besenbacher, *Phys. Rev. B* **56**, 5822 (1997).
- <sup>28</sup>A.V. Ruban, H.L. Skriver, and J.K. Nørskov, *Phys. Rev. B* **59**, 15 990 (1999).
- <sup>29</sup>C. Creemers, *Surf. Sci.* **360**, 10 (1996).
- <sup>30</sup>K. Iwashita, T. Oguchi, and T. Jo, *Phys. Rev. B* **54**, 1159 (1996).
- <sup>31</sup>S. Maat, O. Hellwig, G. Zeltzer, E.E. Fullerton, G.J. Mankey, M.L. Crow, and J.L. Robertson, *Phys. Rev. B* **63**, 134426 (2001).
- <sup>32</sup>R. Hirschl, Y. Jeanvoine, G. Kresse, and J. Hafner, *Surf. Sci.* **482-485**, 712 (2001).
- <sup>33</sup>R. Hirschl and J. Hafner, *Surf. Sci.* **498**, 21 (2002).
- <sup>34</sup>Š. Pick and P. Mikušik, *Phys. Rev. B* **47**, 15 860 (1993).
- <sup>35</sup>P. Oelhafen, in *Glassy Metals II*, Vol. 53 of *Topics in Applied Physics*, edited by H. Beck and H.J. Güntherodt (Springer, Berlin, 1983), p. 283.
- <sup>36</sup>E.K. Hlil, R. Baudoing-Savois, B. Moraweck, and A.J. Renouprez, *J. Phys. Chem.* **100**, 3102 (1996).
- <sup>37</sup>H. Steininger, S. Lehwald, and H. Ibach, *Surf. Sci.* **123**, 264 (1982).
- <sup>38</sup>D.F. Ogletree, M.A. van Hove, and G.A. Somorjai, *Surf. Sci.* **173**, 351 (1986).
- <sup>39</sup>P.J. Feibelman, B. Hammer, J.K. Nørskov, F. Wagner, M. Scheffler, R. Stumpf, R. Watwa, and J. Dumesic, *J. Phys. Chem. B* **105**, 4018 (2001).
- <sup>40</sup>Y. Gauthier, M. Schmid, S. Padovani, E. Lundgren, V. Buš, G. Kresse, J. Redinger, and P. Varga, *Phys. Rev. Lett.* **87**, 036103 (2001).
- <sup>41</sup>R. Hirschl and J. Hafner, *Surf. Sci.* **498**, 37 (2002).
- <sup>42</sup>M. Beutl and J. Lesnik, *Vacuum* **61**, 113 (2001).
- <sup>43</sup>F. Delbecq and P. Sautet, *Chem. Phys. Lett.* **302**, 91 (1999).
- <sup>44</sup>A. Gil and P. Sautet, (unpublished).
- <sup>45</sup>A.P. Graham, A. Menzel, and J.P. Toennies, *J. Chem. Phys.* **111(4)**, 1676 (1999).
- <sup>46</sup>K. Nobuhara, H. Nakanishi, and H. Kasai, *J. Appl. Phys.* **88(11)**, 6897 (2000).
- <sup>47</sup>R.A. Olsen, G.J. Kroes, and E.J. Baerends, *J. Chem. Phys.* **111(24)**, 11155 (1999).
- <sup>48</sup>W. Dong, V. Ledentu, P. Sautet, A. Eichler, and J. Hafner, *Surf. Sci.* **411**, 123 (1998).
- <sup>49</sup>M. Eder, K. Terakura, and J. Hafner, *Phys. Rev. B* **64**, 115426 (2001).
- <sup>50</sup>P. Jiang, M. Zappone, and S.L. Bernasek, *J. Chem. Phys.* **99**, 8126 (1993).
- <sup>51</sup>A. Stibor, G. Kresse, A. Eichler, and J. Hafner, *Surf. Sci.* **507-510**, 99 (2002).
- <sup>52</sup>A. Stibor, Master's thesis, Universität Wien, 2001.
- <sup>53</sup>D. Spišák and J. Hafner, *Phys. Rev. B* **64**, 205422 (2001).
- <sup>54</sup>V. Pallassana and M. Neurock, *J. Catal.* **191**, 301 (2000).